Updated parameters of 1743 open clusters based on *Gaia* DR2

W. S. Dias,[1][*] H. Monteiro,[1] A. Moitinho,[2] J. R. D. Lépine,[3] G., Carraro,[4] E. Paunzen,[5] B. Alessi[6] and L. Villela[1,7]

[1]*Instituto de Física e Química, Universidade Federal de Itajubá, Av. BPS 1303 Pinheirinho, 37500-903 Itajubá, MG, Brazil*
[2]*CENTRA, Faculdade de Ciências, Universidade de Lisboa, Ed. C8, Campo Grande, 1749-016 Lisboa, Portugal*
[3]*Universidade de São Paulo, Instituto de Astronomia, Geofísica e Ciências Atmosféricas, São Paulo, SP, Brazil*
[4]*Department of Physics and Astronomy, University of Padova, Vicolo dell'Osservatorio 3, I-35122 Padova, Italy 0000-0002-0155-9434*
[5]*Departament of Theoretical Physics and Astrophysics. Marsaryk University. Brno, Czech Republic*
[6]*Av. Eng. Antônio Heitor Eiras Garcia 1236, apto 142. Bairro Jardim Esmeralda CEP 05588001 São Paulo, SP, Brazil*
[7]*Departamento de Engenharia Elétrica, Universidade Federal do Espírito Santo, Av. Fernando Ferrari, 514, Campus Universitário de Goiabeiras, 29075-710 Vitória, ES, B*

ABSTRACT

In this study we follow up our recent paper (Monteiro et al. 2020) and present a homogeneous sample of fundamental parameters of open clusters in our Galaxy, entirely based on *Gaia* DR2 data. We used published membership probability of the stars derived from *Gaia* DR2 data and applied our isochrone fitting code, updated as in Monteiro et al. (2020), to G_{BP} and G_{RP} *Gaia* DR2 data for member stars. In doing this we take into account the nominal errors in the data and derive distance, age, and extinction of each cluster. This work therefore provides parameters for 1743 open clusters and, as a byproduct, a list of likely not physical or dubious open clusters is provided as well for future investigations. Furthermore, it was possible to estimate the mean radial velocity of 831 clusters (198 of which are new and unpublished so far) using stellar radial velocities from *Gaia* DR2 catalog. By comparing the open cluster distances obtained from isochrone fitting with those obtained from a maximum likelihood estimate of individual member parallaxes, we found a systematic offset of (-0.05 ± 0.04) mas.

Key words: Galaxy: open clusters and associations: general

1 INTRODUCTION

Open clusters (OCs) constitute a privileged class of objects for investigating a range of astronomical topics, from Galactic structure and dynamics, to the formation, structure, and evolution of stars and stellar systems, and are steps in the cosmic distance ladder. Their positions, distances, proper motions and radial velocities, can in general be determined with better precision than those of individual stars, especially for distant objects. Most importantly, with isochrone fitting, their ages can be determined over a broad range with a precision not at reach for most other astronomical objects.

Since the classic works of Becker & Fenkart (1970) and Janes & Adler (1982) OCs have played an important role in revealing the structure and evolution of our Galaxy. Some more recent studies include the tracing of spiral arms (Moitinho et al. 2006; Vázquez et al. 2008; Bobylev & Bajkova 2014), the spiral pattern rotation speed and corotation radius (Dias et al. 2019), the metallicity gradient (Lépine et al. 2011; Donor et al. 2020), the Galactic warp (Vázquez et al. 2008; Cantat-Gaudin et al. 2020) and the location of the Sun with respect to Galactic plane (Cantat-Gaudin et al. 2020). A review of pre-*Gaia* Galactic structure results with OCs can be found in Moitinho (2010). The most widely used catalogs of OCs and their fundamental parameters are the *New catalogue of optically visible open clusters and candidates* (Dias et al. 2002b, hereafter DAML) and *The Milky Way Star clusters* (Kharchenko et al. 2013, hereafter MWSC). Recent, pre-*Gaia* examples of OCs used in other topics, such as stellar astrophysics can be found in Georgy et al. (2013), and for constraining the distance scale in An et al. (2007).

The *Gaia* DR2 catalog (Gaia Collaboration et al. 2018a) presents more than 1 billion stars with magnitude $G \leq 21$ with high precision astrometric and photometric data, improving the stellar membership determination and characterisation of thousands of open clusters (Cantat-Gaudin et al. 2018; Soubiran et al. 2018a; Monteiro & Dias 2019; Bossini et al. 2019; Carrera et al. 2019; Monteiro et al. 2020). As a consequence, in addition to the direct contribution to Galactic structure studies *Gaia* has allowed the discovery of hundreds of new OCs (Liu & Pang 2019; Sim et al. 2019; Castro-Ginard et al. 2018, 2019, 2020; Ferreira et al. 2020), to check the reality of doubtful objects (Cantat-Gaudin & Anders 2020), Monteiro & Dias (2019).

Despite the exquisite quality of *Gaia* DR2, the determination of OC parameters has in many cases remained a challenge. On the one hand, the parameter fitting algorithms have to deal with a number of factors, such as degeneracies, that compromise quality

[*] E-mail:wiltonsdias@yahoo.com.br

of the fits over the whole range of parameter space. On the other hand, poor clusters and/or remaining field contamination may lead to ill defined groups. As a result, several clusters observed by Gaia did not have yet their parameters determined with *Gaia* DR2 data, and many others have unreliable determinations.

In Monteiro et al. (2020) we have focused on the determination of the parameters of 45 difficult clusters, left-overs of previous large scale *Gaia* based studies. This study introduced methodological improvements to isochrone fitting, including an updated extinction polynomial for the *Gaia* DR2 photometric band-passes and the Galactic abundance gradient as a prior for metallicity, which led to a successful automatic determination of the fundamental parameters of those clusters.

This paper is a follow-up to Monteiro et al. (2020). Here we employ the updated isochrone fitting procedure in a large scale homogeneous, *Gaia* DR2 based, determination of parameters for 1743 OCs with previous membership determinations. Both papers are part of an ongoing project to bring DAML into the *Gaia* era.

The remainder of this manuscript is organized as follows. In the next section we describe the sample. Section 3 presents the cluster member stars. In Section 4, we present the determination of the OC astrometric parameters and mean radial velocity. In Section 5, we describe our code of isochrone fitting to determine the distances and ages of the clusters. In Section 8, we compare the results obtained from *Gaia* data with those from UBVRI data for a control sample. Sections 9 and 10 are dedicated to compare our values with published ones. Section 11 provides general comments on the results. Section 12 is dedicated to statistics of the parameters determined in previous sections. In Section 13 we compare the distances from isochrone fits and from parallaxes. Finally, in the Section 14 we summarize the results presenting the main conclusions of this work.

2   THE SAMPLE OF OPEN CLUSTERS INVESTIGATED

In this study we investigated 2237 open clusters and present a list of 1743 clusters including the parameters here determined, and their associated uncertainties. The sample is composed of 475 young clusters (log(age) < 7.5 dex), 1075 intermediate age open clusters (log(age) between 7.5 dex and 9.0 dex) and 193 old clusters (log(age) > 9.0 dex). 365 clusters are located within 1 kpc and 1379 farther than 1 kpc. Figures 1 and 2 show the distribution of the sample in the Galaxy. The statistics of the parameters are discussed in the Section 12.

The sample parameters have the main characteristic of being homogeneous since they are determined with the same isochrone fitting method, using the G_{BP} and G_{RP} magnitudes from *Gaia* DR2 catalog.

We also present the mean proper motion and parallax, the number of astrometric member stars, mean radial velocity and the number of stars used to estimate them, the apparent radius r_{50} containing 50% of the identified members, and the maximum radius r_{max}, which is the largest angular distance between the member stars and the central coordinates of each cluster considered as the mean positions in RA and DEC of the member stars. The coordinates are given at epoch J2015.0 (ICRS) as realized by the *Gaia* DR2 catalog.

The table with the cluster's parameters and the tables with *Gaia* DR2 data of each star in the field with stellar membership probability are given electronically at the *Centre de Données Stellaires* (CDS).

In this text a portion of the table with the parameters of the clusters is presented in Table 1 and Table 2.

3   OPEN CLUSTER MEMBERSHIPS

To determine precise fundamental parameters of open clusters it is necessary to know the member stars. With data from the *Gaia* DR2 catalog, astrometric membership determination has become much more precise than using ground-based data (Dias et al. 2018), leading to clearer CMDs and therefore enabling a more precise and reliable parameters' determination.
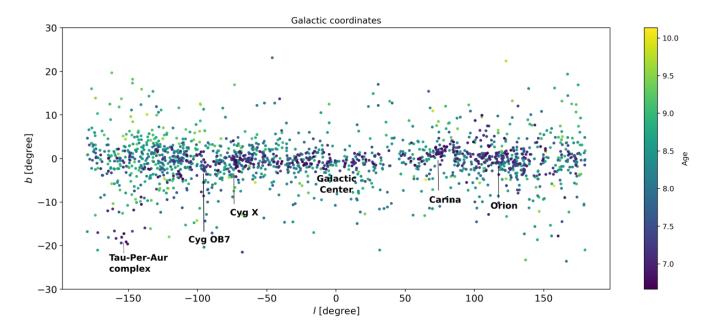
In this work we selected 2237 clusters with published individual stellar membership determined from *Gaia* DR2 astrometric data from the following studies:

• Cantat-Gaudin & Anders (2020), updated Cantat-Gaudin et al. (2018), and estimated stellar membership probabilities for 1867 open clusters applying the UPMASK procedure (Krone-Martins & Moitinho 2014);

• Castro-Ginard et al. (2020) and Castro-Ginard et al. (2019) found hundreds new open clusters looking for overdensities in the astrometric space using DBSCAN and applying the machine learning to the CMD to check if the object is real;

• Liu & Pang (2019) used the Friend of Friend method to find 2443 open clusters and to select their members;

• Sim et al. (2019) found 655 cluster candidates (207 new) by visual inspection of the stellar distributions in proper motion space and spatial distributions in the Galactic coordinates (l, b) space. The members were determined using Gaussian mixture model and mean-shift algorithms;

• Monteiro et al. (2020) investigated 45 open clusters applying the maximum likelihood method to estimate stellar membership in the cluster regions;

• Ferreira et al. (2020) discovered 25 new open clusters and identified the member stars by applying a decontamination procedure to the three-dimensional astrometric space.
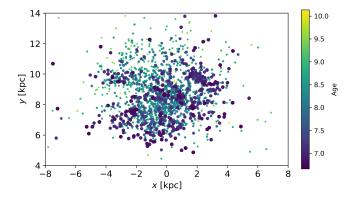
In the works published by Liu & Pang (2019) and Castro-Ginard et al. (2020) the memberships were published as having probability equal to one ($P_i = 1$), for members and zero for non-members. To maintain uniformity with the rest of the sample where individual membership probabilities were available, we recalculated the individual membership probability of the stars (P_i) applying a variation of the classic maximum likelihood approach described in Dias et al. (2014) and Monteiro et al. (2020). In the classic approach, a first step is to determine the bivariate probability density function that represents the distributions of the cluster members and of the field stars in the space formed by proper motions and parallax ($\mu_\alpha cos\delta$, μ_δ, ϖ). The second step is then to use these distributions for assigning cluster/field membership probabilities to the stars under analysis. In the variation here employed, we used the stars reported as members ($P_i = 1$) in Liu & Pang (2019) and Castro-Ginard et al. (2020) to directly estimate the shapes of the membership probability density functions in proper motion and parallax space, and from there proceed to the membership determinations.

This procedure provided individual stellar membership probabilities and allowed us to improve the cluster signature in several CMDs, as shown in Figure 3 for the case of UBC 591.
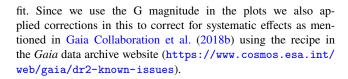
Before using the photometric data we apply filters according to Gaia Collaboration et al. (2018b), to guarantee that only stars with good astrometric solutions are used in the isochrone

Figure 1. Galactic distribution of the 1743 open clusters analysed in this work. The plot present the clusters in Galactic coordinates with the main regions of star formation highlighted. The color is proportional to the age in the sense blue is young, green is intermediate age and yellow is old.
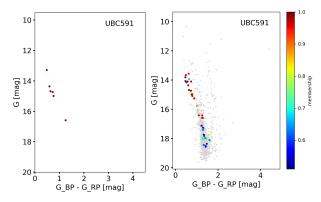

Figure 2. Distribution of the 1743 clusters in the plane x-y. The Galactic Centre at (0,0) as reference and the x−axis pointing to the Galactic rotation direction. The rotation is clockwise or the vector angular velocity is perpendicular to the x˜y plane pointing in the direction of the paper. The y−axis positive points towards the Galactic anticentre and the Sun is situated at (0,8.3) kpc position.
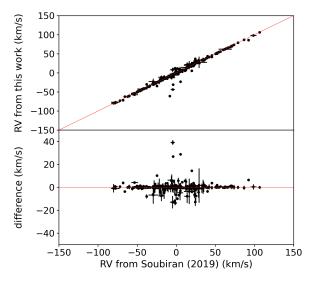

Figure 3. Comparison of the members of the open cluster UBC 591 from Cantat-Gaudin & Anders (2020) (left plot) and from the recalculated memberships from this work (right plot). The stellar membership is proportional to the color, in the sense redder color represent higher membership probability.

fit. Since we use the G magnitude in the plots we also applied corrections in this to correct for systematic effects as mentioned in Gaia Collaboration et al. (2018b) using the recipe in the *Gaia* data archive website (https://www.cosmos.esa.int/web/gaia/dr2-known-issues).

4 PARALLAX, PROPER MOTION AND RADIAL VELOCITY OF THE CLUSTERS

We used the stars with membership probability greater than 0.50 to estimate mean proper motion, parallax and radial velocity of the clusters. For proper motion and parallax we adopted the simple mean, however, to accommodate different numbers of measure-

ments and also measurements with different errors, the mean radial velocity of each open cluster was obtained by weighting with the number of measurements and the error of a single measurement, as used in Dias et al. (2014) following the recipe of Barford (1967). Before computing the mean we applied a 3σ outlier rejection of the radial velocity values. For mean proper motion and parallax, the standard deviation (1σ) was adopted to represent the error.

As we use only the clusters with member stars derived from *Gaia* DR2 data, this was a limiting criterion, since the *Gaia* DR2 catalog gives radial velocity for stars with $G \leq 12$. Even so, mean radial velocity was estimated for 831 open clusters of which 198 had no previous published estimates, of which 106 from Liu & Pang (2019), 81 from the work of Castro-Ginard et al. (2020), 1 from Sim et al. (2019), 7 from Monteiro et al. (2020), 2 from Cantat-Gaudin

Figure 4. Comparison of the mean radial velocity for 229 open clusters in common with Soubiran et al. (2018b). The mean difference is 0.4 km s^{-1} with standard deviation of 5.9 km s^{-1} in the sense literature minus our value.

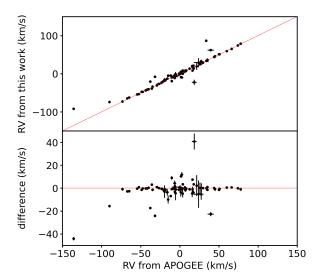**Figure 5.** Comparison of the mean radial velocity for 79 open clusters in common with Carrera et al. (2019). The mean difference is -2.0 km s^{-1} with standard deviation of 10.4 km s^{-1} in the sense literature minus our value.

et al. (2018) and 1 from Ferreira et al. (2020). In Figures 4, 5 and 6 we check our mean radial velocities against the values derived by Soubiran et al. (2018b), Carrera et al. (2019) and Tarricq et al. (2020), all determined using membership from Cantat-Gaudin et al. (2018) and data from *Gaia* DR2 and from APOGEE (Majewski et al. 2017) and GALAH (De Silva et al. 2015) in the case of Carrera et al. (2019). The differences of 229 clusters with Soubiran et al. (2018b) gives a mean of 0.4 km s^{-1} with standard deviation of 5.9 km s^{-1} and the differences of 79 clusters with Carrera et al. (2019) gives a mean of -2.0 km s^{-1} with standard deviation of 10.4 km s^{-1}, and considering 631 open clusters in common with Tarricq et al. (2020) we obtain a mean of 0.4 km s^{-1} with standard deviation of 7.0 km s^{-1}. All the values we calculated in the sense literature minus our result.

As for the comparison between our results and those published, there are 5 open clusters with differences which exceed 3σ. For clusters Alessi 19, Harvard 16, IC 1311, NGC 1027 our values differ with the Soubiran et al. (2018b). The authors used four member stars for Alessi 19 and one member star for the other clusters. For Trumpler 3 our value differs from the Carrera et al. (2019), which used radial velocity from APOGEE DR14 of four members. The differences can be explained by the fact that different studies use different ways of calculating mean radial velocity (weighted or not, with rejection or not). Thus, despite the works being based on memberships from Cantat-Gaudin & Anders (2020), either not exactly the same stars were used or different was the way they were analyzed.
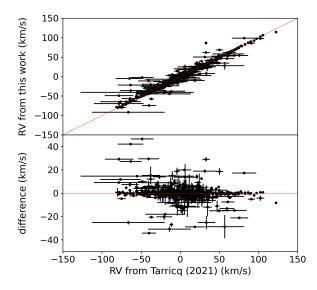
In Table 1 we present a portion of the results giving the mean proper motion, mean parallax and mean radial velocity with the respective errors represented by the one standard deviation. In the table are also given the number of cluster members, the equatorial coordinates (α, δ) and the radius (r_{50}) of each cluster.

5   PARAMETERS FROM THE ISOCHRONE FITS

The parameters distance, age, and A_V of the clusters were obtained by fitting theoretical isochrones to *Gaia* DR2 G_{BP} and G_{RP} photometric data, applying the cross-entropy continuous multi-extremal

Figure 6. Comparison of the mean radial velocity for 631 open clusters in common with Tarricq et al. (2020). The mean difference is 0.4 km s^{-1} with standard deviation of 7.0 km s^{-1} in the sense literature minus our value.

optimization method (CE), which takes into account the astrometric membership of the star as well the nominal errors of the data. It is exactly the same code used in Monteiro et al. (2020) and to avoid being repetitive, we opted to present a general description in this text.

Basically, the CE method involves an iterative statistical procedure where the following loop is done in each iteration:

(i) random generation of the initial sample of fit parameters, respecting predefined criteria

(ii) selection of the 10% best candidates based on calculated weighted likelihood values

(iii) generation of random fit parameter sample derived from a new distribution based on the 10% best candidates calculated in the previous step

(iv) repeat until convergence or stopping criteria reached.

Table 1. A portion of the table of the results of mean astrometric parameters obtained using the *Gaia* DR2 stellar proper motion and parallaxes. The meaning of the symbols are as follows: RA and DE are the central coordinates of the clusters; r_{50} is the radius in which half of the identified members are located; N is the number of cluster stars; $\mu_\alpha\cos\delta$ and μ_δ are the proper motion components in mas yr^{-1}; σ is the dispersion of cluster stars' proper motions; ϖ is the mean parallax of the cluster and $\sigma\varpi$ is the dispersion of the mean parallax. RV and σRV are the mean and 1σ dispersion radial velocity obtained for the cluster using *Gaia* DR2 data.

Name	RA	DE	r_{50}	N	$\mu_\alpha\cos\delta$	$\sigma_{\mu_\alpha\cos\delta}$	μ_δ	σ_{μ_δ}	ϖ	σ_ϖ	RV	σ_{RV}	N
	[deg]	[deg]	[deg]		[mas yr^{-1}]	[mas yr^{-1}]	[mas yr^{-1}]	[mas yr^{-1}]	[mas]	[mas]	[$km.s^{-1}$]	[$km.s^{-1}$]	
Alessi 1	151.6211	49.5407	0.237	48	6.550	0.152	-6.252	0.293	1.396	0.063	-3.343	1.024	11
Alessi 10	35.3246	-10.5442	0.272	73	1.456	0.242	-7.844	0.273	2.227	0.087	-12.671	1.819	6
Alessi 12	308.3153	23.9029	0.660	313	4.339	0.311	-4.650	0.222	1.825	0.098	-3.374	2.662	25

Our method uses a synthetic cluster obtained from an isochrone, sampling from a pre−defined initial mass function (IMF), randomly generating a number of stars in the mass range of the original isochrone.

The code interpolates the Padova (PARSEC version 1.2S) database of stellar evolutionary tracks and isochrones (Bressan et al. 2012), which uses the *Gaia* filter passbands of Maíz Apellániz & Weiler (2018), scaled to solar metal content with $Z_\odot = 0.0152$. The grid used is constructed from isochrones with steps of 0.05 in $log(age)$ and 0.002 in metallicity. A search for the best solutions is performed in the following parameter space:

- age: from log(age) =6.60 to log(age) =10.15 dex;
- distance: from 1 to 25000 parsec;
- A_V: from 0.0 to 5.0 mag;
- $[Fe/H]$: from -0.90 to +0.70 dex

To account for the extinction coefficients dependency on colour and extinction due to the large passbands of *Gaia* filters, we used the most updated extinction polynomial for the *Gaia* DR2 photometric band-passes, as presented in detail by Monteiro et al. (2020).

While the isochrones used are provided as a function of $[M/H]$, in this work we assume $[M/H] = [Fe/H]$. The assumption is justified by considering the relation from (Salaris & Cassisi 2006) which gives $[m/H] \sim [Fe/H]+log(0.694f_\alpha+0.306)$, where $f_\alpha = 10^{[\alpha/Fe]}$. From (Tolstoy et al. 2009, their Fig. 11), we can see that for the range of $[Fe/H]$ in our grid, $[\alpha/Fe]$ is mostly under 0.1. This implies that for most clusters in our sample the assumption is adequate and any difference should be within the uncertainties. As an example of extreme values, we consider the cluster Messier 11 (also catalogued as NGC 6705) which is known to be α-enhanced with $[\alpha/Fe] \sim 0.13-0.17$ (Casamiquela et al. 2018), which would give $[M/H] \sim [Fe/H] + 0.07$, so there may be some effect for the older clusters. As it will be shown later, apart from a few cases, most of the clusters in this work have $[Fe/H] < 0.5$.

In this work, as in Monteiro et al. (2020) we used priors in distance, [Fe/H] and A_V, adopting the prior probability for each parameter given by $P(\mathbf{X}) = \prod_{n=0}^{n} P(X_n)$. For distance we use $\mathcal{N}(\mu, \sigma^2)$ obtained with Bayesian inference from the parallax (ϖ) and its uncertainty (σ_ϖ) and the variance (σ^2) is obtained from the distance interval calculated from the inference using the uncertainty as $1\sigma_\varpi$. The prior in A_V is also adopted as a normal distribution with μ and variance (σ^2) for each cluster taken from the 3D extinction map produced by Capitanio et al. (2017)[1]. The prior for [Fe/H] was estimated from the Galactic metallicty gradient published by Donor et al. (2020). For age there is no prior so we adopt $P(X_n) = 1$.

In our code we adopt a likelihood function given in the usual manner for the maximum likelihood problem as

$$\mathcal{L}(D_N|\mathbf{X}) = \prod_{i=1}^{N} \Phi(I(\mathbf{X}), D_N) \times P_i, \qquad (1)$$

where $\mathbf{X}$ is the vector of parameters (Av, distance d, age $log(age)$ and $[Fe/H]$) that define the maximum $\mathcal{L}$ and N the number of randomly generated, independent sets of model parameters. P_i is the membership probability of the star.

The likelihood function above is used to define the objective function ($S(\mathbf{X}) = -log(P(\mathbf{X}) \times \mathcal{L}(D_N|\mathbf{X}))$) of the optimization algorithm that define a given isochrone $\mathbf{I_N}$. The optimization is done with respect to N.

Finally, our method does not take into account the differential extinction in clusters. The grid of PARSEC isochrones does not include ages younger than ~ 4 Myr ($log(age) = 6.60$ dex) and therefore is not suited for pre-main sequence evolutionary phases where this effect is expected to be large.

In any case, when we look at the results obtained for clusters with known differential extinction, we get good agreement with the literature values. We have 18 clusters from DAML catalog for which we know there is differential extinction. When comparing the results for these objects we find the following mean and standard deviation differences: distance = (-0.056 ± 0.428) kpc, $log(age) = (0.21 \pm 0.42)$ dex, $Av = (0.03 \pm 0.29)$ mag and $[Fe/H] = (0.14 \pm 0.17)$ dex.

Considering the comparison between our results and those from DAML there is no indication of any systematic trend in Av assuring that both sets agree within the uncertainties. The biggest discrepancies are in age which is expected since all of the most discrepant objects are young clusters with the typical problems of poorly defined turn-off, poor membership estimation, and small number of members.

In Table 2 we present a portion of the results obtained by the CE.
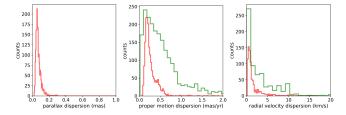
6 INTERNAL UNCERTAINTIES

Figure 7 shows the distribution of the uncertainties in mean parallax, mean proper motion and mean radial velocity, determined in this study. The average uncertainties for the sample are about 0.28 mas yr^{-1} in proper motion, 0.07 mas in parallax and 1.60 km s^{-1} in radial velocity. The figure also displays the distributions of the corresponding uncertainties listed in DAML, showing that this work brings a clear improvement.

The uncertainties of the parameters determined from the isochrone fitting, were estimated applying a Monte-Carlo re-sampling of the member stars with replacement (bootstrapping).

[1] The 3D extinction map is available online at https://stilism.obspm.fr/

Table 2. A portion of the fundamental parameters obtained from the isochrone fits is given.

Name	$dist$	σ_{dist}	$log(age)$	$\sigma_{log(age)}$	$[Fe/H]$	$\sigma_{[Fe/H]}$	A_V	σ_{A_V}
	[pc]	[pc]	[dex]	[dex]	[dex]	[dex]	[mag]	[mag]
Alessi 1	681	15	8.993	0.045	-0.109	0.132	0.416	0.150
Alessi 10	445	9	8.547	0.131	0.019	0.076	0.496	0.066
Alessi 12	539	10	8.195	0.127	-0.023	0.079	0.248	0.087

Figure 7. Distribution of the uncertainty of the parallax, proper motion and radial velocity determined in this study (red color). The uncertainty of proper motion and and radial velocity distributions are compared with those from DAML which are presented in green.

Figure 8. Distribution of the uncertainty of the distance, log(age) and A_V determined in this study.

The synthetic clusters were also re-generated in each run. The final parameters and their uncertainties were estimated as the mean and one standard deviation of ten runs.

The distribution of the uncertainties of the derived parameters are given in Figure 8. Figure 9 presents the internal uncertainties as a function of the parameters. The derived parameters and their uncertainties are given in Table 2, available electronically.

7   THE EFFECT OF THE PRIORS

To assess how much the priors constrain the results we took the sample of 67 clusters with metallicity determinations for high resolution spectroscopy compiled by Monteiro et al. (2020, table A.1). The sample covers practically the full range in distance, age and A_V as well in metallicity.

We start by comparing the values of the parameters obtained from the isochrone fit with the values of the priors. Figure 10 shows how the prior in the distance is very restrictive, which reflects our trust on the quality of Gaia parallaxes. The prior in [Fe/H] is moderately restrictive. Because the fits are less sensitive to metallicity, this avoids solutions with extreme values of metallicity while allowing for reasonable uncertainty in the metallicity gradient. Finally the prior in the A_V is shown to be clearly non restrictive, which reflects our lower trust in the extinction model as well as our high trust that the data is sensitive enough to this parameter as verified in Monteiro et al. (2020). These considerations are also expressed in the correlation coefficients between the parameters obtained from the

isochrone fits and the values of the priors, which are 0.95, 0.68 and 0.30 for distance, [Fe/H] and A_V, respectively.

We now present in Figure 11 the comparison of the parameters from the isochrone fits with and without the adopted priors. The correlation of the parameters obtained with and without priors are 0.99, 0.98, 0.97 and 0.33 for distance, age, A_V and [Fe/H], respectively.

The differences between the parameters determined with priors and with no priors are in agreement considering the errors as pointed by the mean differences 0.010 kpc in distance, 0.014 dex in log(age), -0.069 mag in A_V and 0.032 dex in [Fe/H] with standard deviation of 0.187 kpc, 0.142 dex, 0.234 mag, 0.237 dex.

Another indication of how much the priors constrain the results is given by the ratio of the width of the prior distribution, σ_{prior}, to the error of the respective parameter (σ_{dist}, σ_{Av}, $\sigma_{[Fe/H]}$) estimated from the isochrone fit with no priors. These ratios are presented in Figure 12. Note that the errors in the parameters estimated without prior are essentially a measure of the dispersion of the likelihood distribution. In this sense we can say that priors restrict results if the ratio is much less than the likelihood dispersion. In other words, a ratio $\sigma_{prior-parameters}/\sigma_{parameter}$ greater than 1 means that a prior is not very restrictive and smaller than 1 that it is more restrictive.

8   THE CONTROL SAMPLE

In the analysis of UBVRI data the U band clearly improves the reliability of the parameters estimated for the open clusters, since it removes the spectral-type/reddening degeneracy in the color−color diagrams. In this way the agreement of the results derived from *Gaia* DR2, in this study using G_{BP} and G_{RP} magnitudes, with those from the literature obtained with U filter is a quality indicator of the efficiency in the determination of cluster's parameters.

To perform this check we use high quality homogeneous UB-VRI photometry of 20 open clusters published by Moitinho (2001).

Each star observed by Moitinho (2001) was cross-matched with those from Cantat-Gaudin & Anders (2020) for assigning *Gaia* based memberships to the UBVRI data. In the procedure we used the SKY algorithm from TOPCAT (Taylor 2005) to cross-match the data with coordinates in the J2000 equinox and same epoch. Note that the different number of stars in each sample is due to the smaller field of view of the ground-based observations.

To fit the isochrones to the UBVRI data we used our code and the same procedure adopted for the *Gaia* isochrone fitting described in Section 5, including the prior in distance and [Fe/H] and adopting the reddening law from Cardelli et al. (1989) as used in Dias et al. (2018). So, the method applied to both data samples is as similar as possible.

In Figure 13 we present the CMDs and color−color diagram for NGC 2571 as examples of the results obtained both using *Gaia* G_{BP} and G_{RP} and UBVRI data. In Figure 14 and Table 3 we show the comparison of the values of the parameters obtained with our code applied to the *Gaia* and UBVRI data.
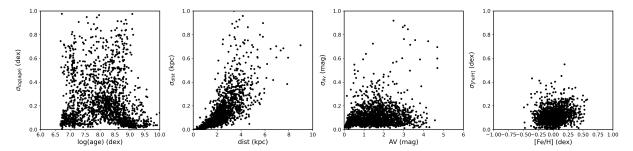
Figure 9. Distribution of the internal uncertainties for the parameters from isochrone fit determined by the cross-entropy method.
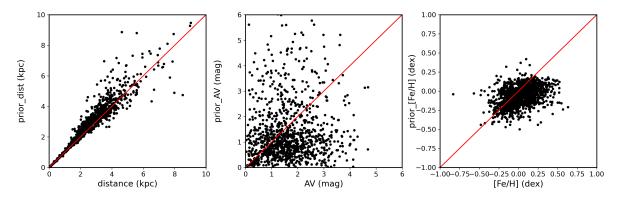

Figure 10. Comparison of the values of the parameters obtained from the isochrone fit with the values of the priors used.
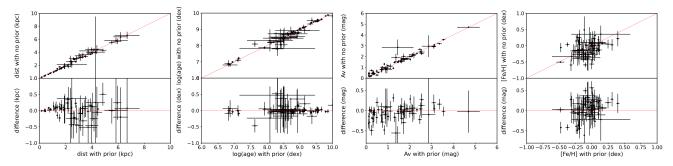

Figure 11. Comparison of the values of the parameters obtained from the isochrone fit with and without priors.

The differences between the parameters determined from UB-VRI data and from *Gaia* data are in agreement at a 3σ level and considering the errors indicated by the mean differences (0.005 dex in log(age), -59 pc in distance, -0.007 mag in A_V and 0.11 dex in $[Fe/H]$) with root mean square difference (0.302 dex in log(age), 218 pc in distance, 0.099 mag in A_V and 0.16 dex in $[Fe/H]$), in the sense of results from *Gaia* data minus UBVRI data.

However, we can notice some differences at the 1σ level. The most discrepant cases are clusters with poorer fits in *Gaia* DR2 data. The difference in distance and/or age of OCs Haffner 19, NGC 2311, NGC 2367, NGC 2401 occurs due to the poorly defined main sequence (MS) and/or turn-off (TO) in *Gaia* DR2 data. The differences in distance for NGC 2425 and NGC 2635 can be explained by the differences in A_V and metallicity. For the distant clusters NGC 2401 and Haffner 19 the poorer parameters are in line with what is expected from the internal uncertainties shown in Figure 9. NGC 2367 is a very young cluster with sparse and poorly defined sequence.

The $[Fe/H]$ values are presented for comparison purposes and should be considered with caution. As noted in Monteiro et al.

(2020) and in Section 7, the isochrone fits employ a moderately restrictive metallicity gradient prior. Thus, while individual metallicities are reasonable estimates, as a group they may be biased towards the Galactic metallicity gradient used as prior. For A_V, the results are hardly affected by the prior which is mostly non-restrictive.

The results for the clusters in this control sample from Moitinho (2001), together with the extensive validation performed in Monteiro et al. (2020) indicate that the parameters here obtained with *Gaia* G_{BP} and G_{RP} data are reliable. Still, it should be kept in mind that the analysis has been performed with a small number of clusters, with different numbers of stars used in each data set due to the different sizes of the fields. We note that the results of the isochrone fit depend on the number of stars used and clearly in the *Gaia* data there are many more stars than in the UBVRI data considered in this comparison. On the other hand, UBVRI photometry can better constrain the results since it is not so affected by degeneracies in the parameter determinations. We also tested the isochrone fitting with UBVRI data using no prior in distance and $[Fe/H]$. The results of the parameters agree within the estimated errors showing no statistical distinction.
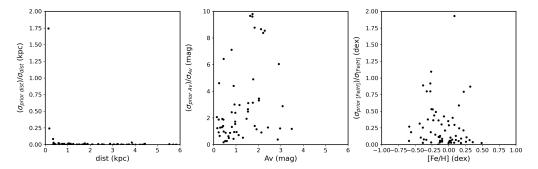
Figure 12. Ratio of the width of the prior distribution, σ_{prior}, to the error of the respective parameter: σ_{dist} (left), σ_{Av} (middle), $\sigma_{[Fe/H]}$ (right).

In the next Sections we present more evidence supporting that the results obtained in this work are reliable and improve upon published ones that used *Gaia* DR2 data .

9   COMPARISON WITH THE LITERATURE AFTER *GAIA*

The large scale results of cluster parameters, mainly distance and age, published after the *Gaia* DR2 catalog can briefly summarized as follows:

- Cantat-Gaudin et al. (2020) estimate the distance, age, and interstellar reddening for 1867 clusters using artificial neural networks applied to G, G_{BP} and G_{RP} magnitudes of member stars brighter than $G = 18$
- Bossini et al. (2019) estimated age, distance modulus and extinction for a sample of 269 open clusters applying BASE-9 (von Hippel et al. 2006), to fit stellar isochrones on the observed G, G_{BP} and G_{RP} magnitudes of the high probability member stars from Cantat-Gaudin et al. (2018)
- Liu & Pang (2019) used its own algorithm to automatic isochrone fitting applied to CMD of 2443 cluster candidates, considering stars with $G \leq 17$
- Sim et al. (2019) used least-squares fitting of isochrones to CMDs, considering the mode of distribution of the parallaxes of the member stars as cluster distance. The authors used for interstellar reddening E($G_{BP} - G_{RP}$) and the extinction in the G band, A_G, using the extinction values from *Gaia* DR2.

Figure 15 gives the comparison of the parameters for 1259, 257, 149 and 128 open clusters in common with Cantat-Gaudin et al. (2020), Bossini et al. (2019), Liu & Pang (2019) and Sim et al. (2019), respectively.

The comparisons should be made carefully since the mentioned studies determine open cluster parameters through isochrone fitting using different methods and strategies. Although the works cited used PADOVA isochrones (Bressan et al. 2012), scaled to solar metal content with $Z_\odot = 0.0152$, Cantat-Gaudin et al. (2020), Bossini et al. (2019) and Sim et al. (2019) opted to use a fixed metallicity while Liu & Pang (2019) considered metallicity as a free parameter in the isochrone fit.

The study of Liu & Pang (2019) uses stars with $G \leq 17$ and the other works used stars limited to $G = 18$. Since we used the stellar membership previously published we follow the same magnitude cut-offs which imposes limitations to obtain adequate results for more distant open clusters due to the low sampling of the main sequence. For that reason the oldest known open clusters as Berkeley 15 and ESO 393 12 and many others are not present in our sample.

The comparison of our values with those derived by Cantat-Gaudin et al. (2020) shows systematic trends in A_V and distance, in the sense of our A_V being larger and distance being smaller than those of Cantat-Gaudin et al. (2020). Despite the large dispersion ($\sigma = 0.33$) no trend in age is detected. The same systematic trends in A_V and distance can be seen in the comparison with the values by Bossini et al. (2019). While all studies used the same member stars, deviations are expected due to differences in the methods, which include different extinction laws and priors in Bossini et al. (2019) and Cantat-Gaudin et al. (2020).

Regarding the discrepancies in ages, we found 22 clusters with differences larger than 3σ. The objects are presented in Table A1. An inspection of the CMDs reveals considerable scatter and/or poor membership determination which lead to poor isochrone fit, mainly due to lack of clear turn-off, which justifies the differences obtained between our parameters and those from Cantat-Gaudin et al. (2020). We expect that these cases can have better results with the catalog *Gaia* EDR3.

The comparison with Sim et al. (2019) shows no expected systematic trend in distances. This is because their method estimates the distances from the mode of the parallaxes of the members corrected of zero-point offset of -0.029 mas from Lindegren et al. (2018). The authors used the colour excess E($G_{BP} - G_{RP}$) and absorption A_G from the Gaia DR2 catalog to estimate the interstellar extinction in their isochrone fitting. However, Arenou et al. (2018) have shown that the extinction values published in Gaia DR2 are not very reliable and even exhibit large spreads within the same OC. These artifacts in interstellar extinction, the adoption of solar metallicity as well as some possible bias in distance may have affected the ages determined by Sim et al. (2019). A more detailed analysis would be needed to understand the contribution of each factor to the difference in the estimated ages, but that is beyond the scope of this study.

Regarding the comparison with Liu & Pang (2019), we note that there is no good agreement. The plot of the comparison of [Fe/H] shows steps of 0.25 dex used by the authors in the isochrone fit. Possibly as happened with the results of Sim et al. (2019), the values of the metallicity may have affected the ages determined by the authors. Note that since class 3 objects in Liu & Pang (2019) contains very young clusters with log(age)≤6.8 dex, the highest density in the young clusters shown in the plot of age comparison is expected as pointed by Liu & Pang (2019, their Fig. 7).

Finally, we quantitatively evaluate the reliability of the parameters obtained from the isochrone fit by comparing them with the data. For this we use as a figure of merit the likelihood provided in equation 1. According to this definition the best fit is the one which maximizes the likelihood, or as in our algorithm, minimizes the ob-
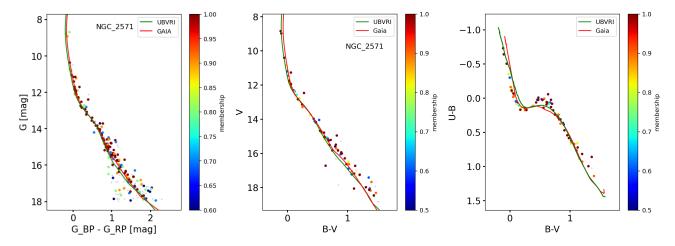
Figure 13. Comparison of the parameters obtained from *Gaia* data (red isochrones) and from UBVRI data (green isochrones) for NGC 2571. The memberships from Cantat-Gaudin & Anders (2020) are proportional to the color in the sense of redder indicating higher membership probability.
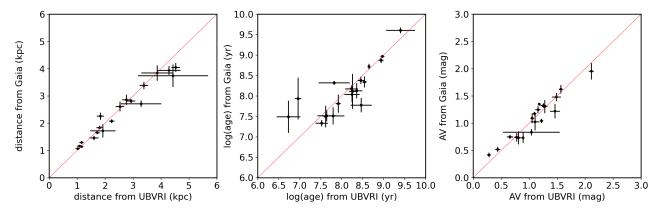

Figure 14. Comparison of the parameters obtained from *Gaia* G_{BP}, and G_{RP} and UBVRI data for a sample of 20 open clusters from Moitinho (2001).

Table 3. Parameters obtained for 20 clusters with UBVRI data from Moitinho (2001). Columns two to six list the parameters determined using *Gaia* G_{BP}, and G_{RP} data. Columns seven, eight and nine list the values obtained from UBVRI data.

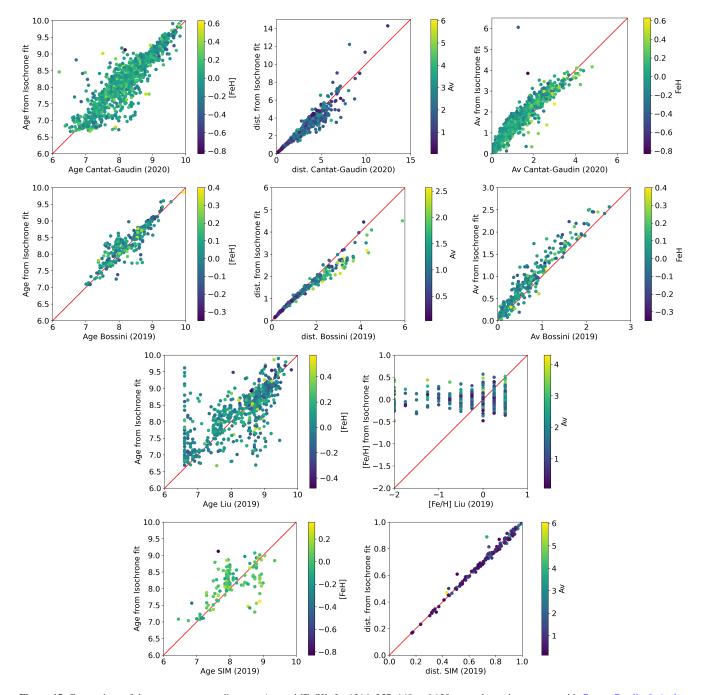|	Results from *Gaia* data				Results from UBVRI data			
Cluster	Distance	log(Age)	A_v	$[Fe/H]$	Distance	log(Age)	A_v	$[Fe/H]$
	[pc]	[dex]	[mag]	[dex]	[pc]	[dex]	[mag]	[dex]
Haffner 16	2862 ± 186	7.513 ± 0.210	0.750 ± 0.037	−0.160 ± 0.127	2759 ± 154	7.794 ± 0.271	0.656 ± 0.055	−0.258 ± 0.113
Haffner 19	3745 ± 413	7.938 ± 0.510	1.221 ± 0.131	−0.210 ± 0.159	4428 ± 1254	6.959 ± 0.076	1.462 ± 0.090	−0.473 ± 0.492
NGC 2302	1162 ± 27	8.038 ± 0.186	0.733 ± 0.119	−0.025 ± 0.043	1084 ± 096	8.245 ± 0.183	0.806 ± 0.059	−0.338 ± 0.127
NGC 2309	2076 ± 71	8.343 ± 0.136	1.326 ± 0.041	−0.111 ± 0.073	2235 ± 095	8.542 ± 0.053	1.254 ± 0.053	−0.143 ± 0.069
NGC 2311	1839 ± 62	7.777 ± 0.175	1.092 ± 0.091	−0.079 ± 0.057	1801 ± 120	8.465 ± 0.252	1.053 ± 0.031	−0.295 ± 0.106
NGC 2335	1462 ± 82	7.812 ± 0.220	1.480 ± 0.076	−0.071 ± 0.101	1603 ± 163	7.917 ± 0.061	1.486 ± 0.080	0.118 ± 0.239
NGC 2343	1068 ± 36	8.174 ± 0.088	0.743 ± 0.078	0.063 ± 0.110	1018 ± 080	8.236 ± 0.155	0.776 ± 0.045	−0.181 ± 0.082
NGC 2353	1140 ± 16	8.127 ± 0.185	0.522 ± 0.046	−0.055 ± 0.049	1158 ± 058	8.357 ± 0.134	0.437 ± 0.046	−0.104 ± 0.068
NGC 2367	1722 ± 244	7.490 ± 0.394	1.025 ± 0.156	−0.065 ± 0.125	1918 ± 452	6.731 ± 0.282	1.106 ± 0.075	−0.383 ± 0.327
NGC 2383	2815 ± 79	8.382 ± 0.091	1.175 ± 0.031	−0.174 ± 0.043	2925 ± 154	8.454 ± 0.074	1.095 ± 0.033	−0.171 ± 0.100
NGC 2401	3940 ± 165	8.322 ± 0.046	1.044 ± 0.040	−0.168 ± 0.081	4281 ± 417	7.820 ± 0.373	1.220 ± 0.029	−0.346 ± 0.227
NGC 2425	2714 ± 123	9.604 ± 0.071	0.836 ± 0.060	0.047 ± 0.089	3288 ± 726	9.403 ± 0.344	1.038 ± 0.507	−0.314 ± 0.219
NGC 2432	1651 ± 51	8.971 ± 0.031	0.735 ± 0.095	0.014 ± 0.105	1722 ± 080	8.970 ± 0.047	0.891 ± 0.022	−0.183 ± 0.074
NGC 2439	3386 ± 136	7.334 ± 0.081	1.350 ± 0.024	−0.117 ± 0.074	3385 ± 155	7.523 ± 0.147	1.180 ± 0.026	−0.205 ± 0.094
NGC 2453	3842 ± 283	7.498 ± 0.265	1.624 ± 0.079	−0.171 ± 0.063	3865 ± 571	7.617 ± 0.051	1.565 ± 0.034	−0.217 ± 0.318
NGC 2533	2613 ± 180	8.871 ± 0.066	1.307 ± 0.121	−0.103 ± 0.080	2529 ± 151	8.937 ± 0.059	1.277 ± 0.047	−0.261 ± 0.102
NGC 2571	1293 ± 46	7.517 ± 0.138	0.419 ± 0.041	0.058 ± 0.106	1154 ± 076	7.644 ± 0.225	0.280 ± 0.037	−0.118 ± 0.117
NGC 2635	4049 ± 167	8.720 ± 0.066	1.250 ± 0.061	−0.218 ± 0.117	4523 ± 160	8.649 ± 0.030	1.157 ± 0.048	−0.177 ± 0.060
Ruprecht 18	2259 ± 130	8.114 ± 0.427	1.953 ± 0.152	0.123 ± 0.155	1830 ± 130	8.256 ± 0.083	2.110 ± 0.045	−0.500 ± 0.168
Trumpler 7	1546 ± 60	8.185 ± 0.278	1.027 ± 0.141	−0.100 ± 0.083	1439 ± 162	8.052 ± 0.285	0.968 ± 0.198	−0.286 ± 0.198

Figure 15. Comparison of the parameters age, distance, A_V and [Fe/H], for 1216, 257, 149 and 128 open cluster in common with Cantat-Gaudin & Anders (2020), Bossini et al. (2019), Liu & Pang (2019) and Sim et al. (2019), respectively.

jective function constructed from it. Thus, the likelihood-ratio test, or the ratio of the values of the objective function, from two distinct solutions can indicate which was the best.

Since our method uses synthetic clusters obtained from model isochrones, we performed Monte-Carlo runs calculating the value of the likelihood for random samples of generated clusters with a given set of input parameters. The process was performed 100 times and we adopted the mean of the likelihood sample as the final value and 1σ as uncertainty. To calculate the likelihood value from the literature parameters, we use the same data and extinction law provided by Monteiro et al. (2020). In Figure 16 the logarithm of the likelihood values are presented for our sample and those of

Cantat-Gaudin et al. (2020), Bossini et al. (2019), and Sim et al. (2019). The results show that, within our specified constraints and minimization criteria (isochrones, priors, extinction law, etc), we are obtaining the best solution.

10   COMPARISON WITH THE CATALOGS BEFORE *GAIA* DR2

In this section we compare our results with the New Catalog of Optically Visible Open Clusters and Candidates (Dias et al. 2002b) (DAML) and Milky Way Star Cluster catalog (Kharchenko et al.
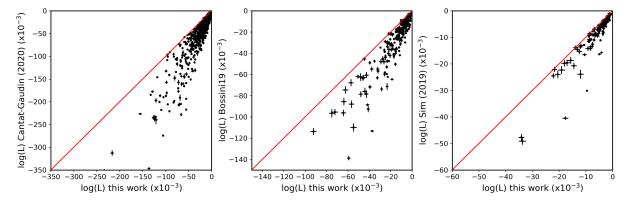
Figure 16. Comparison of the likelihood ($log(\mathcal{L})$) for open clusters in common with Cantat-Gaudin et al. (2020), Bossini et al. (2019), and Sim et al. (2019), respectively.

2013) (hereafter MWSC) both published before *Gaia* DR2 and used in hundreds of works. A detailed discussion of the differences, advantages and disadvantages of both catalogs is presented in Monteiro et al. (2020).

Briefly, the MWSC catalog is based in the PPMXL catalog (Roeser et al. 2010) and 2MASS catalog (Skrutskie et al. 2006) to determine kinematic and photometric membership probabilities for stars in a cluster region. The authors defined a combined stellar membership probability and determined parameters of 3006 clusters using near infra-red J,H and K_s data.

Version 3.5 of DAML presents 2174 clusters with parameters compiled from the literature, giving priority to observational data including the U filter, due to its importance in the determination of the $E(B-V)$ through the color-color diagram which allows more reliable determinations of distances and ages. In the comparison with DAML catalog all results from MWSC catalog were removed.

In Figure 17 we present the comparison of the parameters for 744 and 933 open clusters with DAML and MWSC, respectively. The differences obtained for each parameter are shown in Table 4.

The results of the comparison show the same characteristic scatter and trends seen in the similar comparisons by Monteiro et al. (2020), Cantat-Gaudin et al. (2020) and Bossini et al. (2019). While the Gaia based results represent overall a clear improvement over the pre-Gaia catalogs, it must be noted that distant, more reddened and older clusters are fainter and don't have Gaia based photometry and membership determinations. For those clusters the pre-Gaia catalogs remain useful and the comparisons here presented give an idea of their expected precision.

11 GENERAL COMMENTS

The 1743 open clusters included in this work pass the empirical criteria for bona fide clusters with Gaia proposed by Cantat-Gaudin & Anders (2020) and a visual inspection of the CMD with the fitted isochrone over-plotted. Typical cluster detected in Gaia DR2 show small total proper motion dispersion, clear features in the CMD (e.g. main sequence, turn-off, red clump), 50% of their members are within a radius of 15 pc, parallax dispersion of the member stars adequate to the group's distance, and a minimum number of 10 member stars.

Visual inspection of the CMDs indicates that many clusters detected with Gaia DR2 by Liu & Pang (2019) and some by Castro-Ginard et al. (2020) are dubious or not physical objects although we recalculated the individual membership probability of the stars.

This is in agreement with the original classification by the authors. Liu & Pang (2019) considered 1747 (72%) candidates as class 3 and 127 (5%) as class 2, using as criterion the width of the MS, age and quality of the isochrone fitting. Castro-Ginard et al. (2020) considered 101 (15%) candidates as class B and 235 (36%) as class C, considering the concentration of member stars in the astrometric parameters and the contamination in the CMD. We estimate that objects in class A from Castro-Ginard et al. (2020) and class 1 from Liu & Pang (2019) are likely star clusters candidates while the candidates in the other classes need confirmation.

Figures 18 and 19 show typical cases we found with dubious and non real objects for which our code was unable to obtain reliable solutions. In short, some clusters as UBC 625 and fof sc 2002 have few members and despite the low dispersion in proper motion, the CMDs do not show the typical clear features of a real cluster. Other cases as UBC 649 and fof sc 2213 have CMDs with a gap of more than 1 mag in the possible main sequence of the cluster, that cannot be explained by the theory of stellar evolution. A number of clusters, as fof sc 1605, have very spread MS on the CMD without a feature of a cluster. The list of likely not real open clusters (85 not real and 82 dubious) is given in Tables B1 and B2 for further investigations.

The large number of doubtful cases mainly from Liu & Pang (2019) can be explained as due to objects that are not real open clusters. Figure 20 presents a comparison of the total proper motion dispersion of real open clusters (from Cantat-Gaudin & Anders (2020)) and the sample of the open clusters from Liu & Pang (2019). The figure shows a clear separation of their class 2 (lower isochrone fit quality) and class 3 (lower isochrone fit quality and scattered CMD) samples both with many clusters with total proper motion dispersion greater than their class 1 (higher quality results) and mainly greater than the real clusters from Cantat-Gaudin et al. (2020). On the other hand, Figure 20 shows the same analysis to UBC open clusters considering the classification from Castro-Ginard et al. (2020). Here we note that the majority of cases fall within the proper motion dispersion of real open clusters from Cantat-Gaudin et al. (2020). Although the dispersion of the proper motion is not a definitive proof, it does provide indication that a large proportion of class 2 and 3 objects from Liu & Pang (2019) are not real clusters. We understand that these cases need further confirmation. For this reason we opted to give a list of dubious cases and revisit it in a more detailed study in another work.

Finally, we point out that older and more distant open clusters, such as Saurer 2 presented in Figure 23, do not define clear main sequences with published members and our code results in poor parameter estimates. Nevertheless, the reality of Saurer 2, which
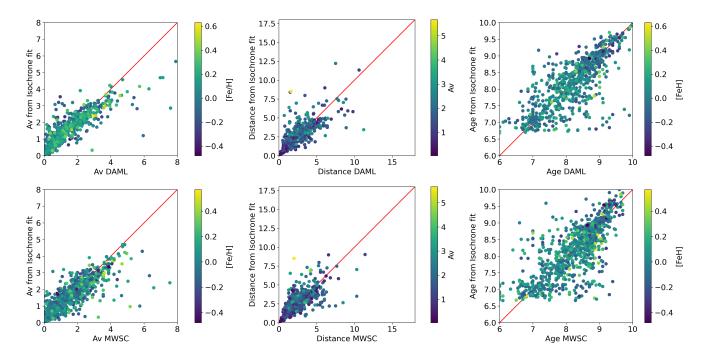
Figure 17. Comparison of the parameters determined in this work with the values published by DAML and MWSC catalogs.

Table 4. Comparison of our results with those published in the literature. In the first column are give the reference. The values in the subsequent columns are in the sense our results minus literature. N is the number of common clusters.

ref	distance [pc]	σdist [pc]	log(age) [dex]	σlog(age) [dex]	A_V [mag]	σA_V [mag]	[Fe/H] [dex]	σ[Fe/H] [dex]	N
DAML	111	1046	-0.048	0.582	0.048	0.920	0.095	0.243	744
MWSC	120	906	-0.088	0.571	-0.033	0.751	0.112	0.256	933
Cantat−Gaudin	-167	414	-0.057	0.384	0.289	0.268			1216
Bossini	-138	262	-0.067	0.250	0.170	0.174			257
Sim	-4	18	-0.089	0.477					128
LP			-0.557	0.896			0.090	0.777	149

DAML = Dias et al. (2002b); MWSC = Kharchenko et al. (2013); Cantat−Gaudin = Cantat-Gaudin et al. (2020); Bossini = Bossini et al. (2019); Sim = Sim et al. (2019); LP = Liu & Pang (2019)

was not discovered based on *Gaia* data, is not in question. This is a case of real cluster that is too faint to have enough *Gaia*DR2 based membership determinations to define a clear CMD sequence. These cases were eliminated from the final list in the visual inspection phase.

12   STATISTICS

Although determinations of distance, extinction, number of members and proper motion dispersion may change using deeper photometric surveys or improved astrometric precision, the statistical description of the results from this work can provide a useful reference, in addition to the bona-fide criteria from Cantat-Gaudin & Anders (2020), for assessing if an object is or not a real OC.

Figure 21 shows the distribution of the parameters of the 1743 open clusters investigated in this study. It is noted that 70% of the clusters have up to 50 members, 90% have total proper motion dispersion less than 0.5 mas yr^{-1} (regardless of the distance) and 99% have a radius smaller than 15 pc (considering r_{50}).

The clusters have distances from the Sun that vary from 47 pc (Melotte 25 = Hyades) to 8978 pc (Tombaugh 2) with 21% of the sample located within 1 kpc from the Sun. The maximum A_V determined in this study was about 6 mag for cluster UPK 402. The range in log(age) is 6.7 dex (FSR 1352) to 10.0 dex (Berkeley 17).

Finally, we also investigated the relations between cluster parameters and distance to the Galactic Center, but no significant correlation was found.

13   COMPARISON OF DISTANCES FROM PARALLAXES AND ISOCHRONE FITING

Studies comparing the distances obtained using *Gaia* DR2 parallaxes with those from other methods show the existence of a systematic offset. The value of the offset ranges from −0.082 mas to −0.029 mas, depending on the objects and the method used, as shown by Arenou et al. (2017).

Stassun & Torres (2018) estimated a systematic offset of (−0.082±0.033) mas using a sample of 158 eclipsing binary. Riess
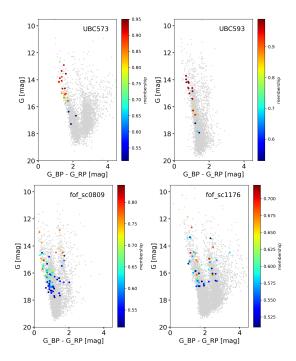
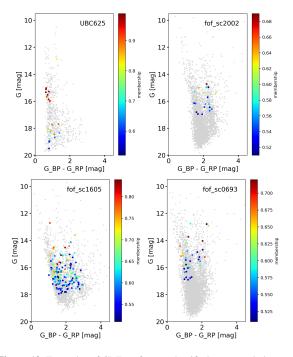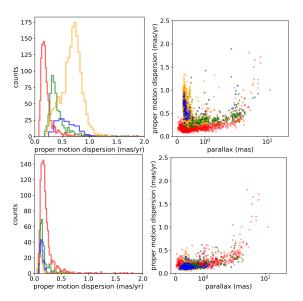**Figure 18.** Examples of CMDs of cases classified as dubious.

Figure 19. Examples of CMDs of cases classified as not real clusters.

Figure 20. Upper panels: Comparison of the total observed proper motion dispersion ($\sqrt{(\mu_\alpha \cos \delta)^2 + (\mu_\delta)^2}$) in mas yr^{-1} of the open clusters from Cantat-Gaudin et al. (2020) (red), Liu & Pang (2019) class 1 (green), class 2 (blue) and class 3 (orange). The plot on the right gives the total observed proper motion dispersion as a function of the cluster mean parallax with the x-axis on a log scale. Bottom panels: the same for open clusters from Castro-Ginard et al. (2020) with color codes for their class A (green), class B (blue) and class C (orange).

et al. (2020) performed a combined analysis of UBVI photometry and Gaia DR2 data with the ASteCA code for inference of cluster parameters and report an offset of −0.026 mas using a sample of 10 clusters.

Figure 22 presents a comparison of the distances determined from isochrone fits and from parallaxes for the 1743 open clusters in this study. The distances obtained from parallaxes were determined with a maximum likelihood estimation assuming a normal distribution for individual member stars and taking into account individual parallax uncertainties. The errors were estimated by considering a symmetric distribution so that $\sigma = r_{95} - r_5/(2 \times 1.645)$, which is equivalent to a 1σ Gaussian uncertainty, where r_5 and r_{95} are the 5th and 95th percentile confidence intervals. To estimate the individual cluster offsets we maximize the following maximum likelihood formulation:

$$\mathcal{L} \propto \prod_{i=1} P(x|d_{iso}, \varpi_i, \sigma_{\varpi_i}) =$$

$$\prod_{i=1} \frac{1}{\sqrt{2\pi\sigma_{\varpi_i}^2}} \exp\left(-\frac{[(\varpi_i + x) - \frac{1}{d_{iso}}]^2}{2\sigma_{\varpi_i}^2}\right) \qquad (2)$$

where $P(x|d_{iso}, \varpi_i, \sigma_{\varpi_i})$ is the probability of obtaining an offset x given the cluster d_{iso}, the distance from the isochrone fit (in kpc), the value of ϖ_i (in mas) for the parallax of cluster member star i and its uncertainty σ_{ϖ_i}. An important assumption here is that the size of the cluster is smaller than its distance and so the procedure will not be ideal for large nearby objects. We have also neglected the correlations between parallax measurements.

With the procedure outlined above we found a global offset of $(−0.05 \pm 0.04)$mas and $(−0.05 \pm 0.03)$mas using the mean and median of the sample of differences, respectively. Our analysis follows the suggestion of Zinn et al. (2019) that the offset may increase with the distances, as can be seen in Figure 22.
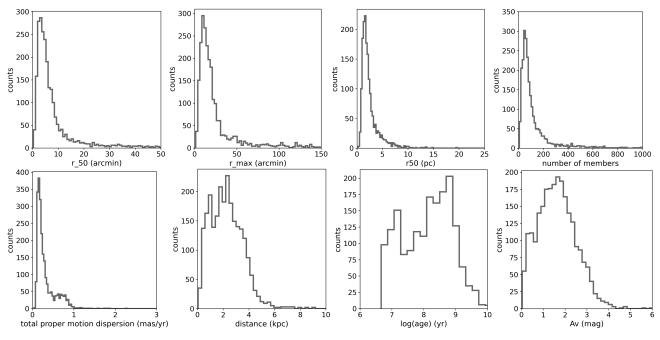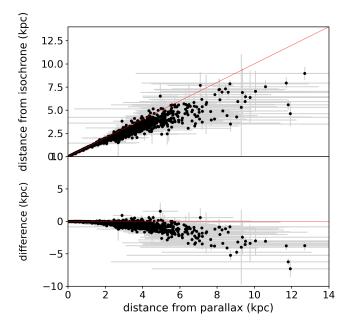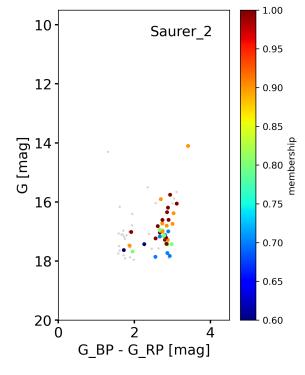
et al. (2018) determined a global offset of (-0.046±0.013) mas using 50 Cepheids. Zinn et al. (2019) finds (-0.0528 ± 0.0024) mas using more than 3000 stars with asteroseismically determined. Kounkel et al. (2018) used 55 young stars with Very Large Baseline Array parallaxes and finds an offset of (-0.074 ± 0.034) mas. A global zero-point of −0.029 mas was found by Lindegren et al. (2018) using the high-precision sample of about 493 thousands quasars. Arenou et al. (2017) presented a residual zero-point in parallaxes of (-0.067 ± 0.120) mas for MWSC and (-0.064 ± 0.170) mas for DAML, comparing the stars in about 200 clusters. Finally, Perren

Figure 21. Distribution of the parameters of the 1743 open clusters presented in this work. r_{50} is the apparent radius containing 50% of the cluster's members and the maximum radius r_{max} is the greatest angular distance between the member stars and the central coordinates of each cluster. The total proper motion dispersion is given by ($\sqrt{(\mu_\alpha \cos \delta)^2 + (\mu_\delta)^2}$).

Figure 22. Comparison of the distances determined from isochrone fits and from parallaxes. The bottom plot shows the difference in distance in the sense distance from isochrones minus from parallaxes as a function of the distance from parallaxes.

Figure 23. Saurer 2 is a typical old and distant cluster for which the data do not define a main sequence and our code fails in the estimation of the parameters.

14   CONCLUSIONS

We presented an update of parameters for 1743 Galactic open clusters from isochrone fits to *Gaia* DR2 data, using the improved extinction polynomial and metallicity gradient prior as presented in Monteiro et al. (2020), and in addition a weak prior in interstellar extinction.

The isochrone fitting code, described in Monteiro et al. (2020, 2017) uses a cross-entropy global optimization procedure to fit isochrones to G_{BP} and G_{RP} magnitudes from *Gaia* DR2 to determine the distance, age, A_V and [Fe/H] of the clusters. The membership probability of stars and their nominal photometric errors

are taken into account. The parameters are given with associated uncertainties, with mean values for the sample are about 170 pc in distance, 0.24 dex in log(age) and 0.12 mag in A_v.

In this study, we used stellar membership probabilities published in the literature. However, for the clusters from Liu & Pang (2019) and Castro-Ginard et al. (2020) the values were recalculated applying a maximum likelihood approach which allowed the construction of clearer CMDs and better weights for the isochrone fitting code.

The mean radial velocities of the clusters were determined from *Gaia* DR2 radial velocities of member stars. In total, radial velocity were calculated for 831 clusters of which 198 had no previous published estimates.

The parameters of the sample indicate that the clusters detected in *Gaia* DR2 50% of their members are within a radius of 15 pc and total proper motion dispersion smaller than $0.5 - 0.8 \; mas \; yr^{-1}$.

Analysis of the differences in distances determined from isochrone fitting and from parallax indicates an offset in the *Gaia* DR2 parallax of (-0.05 ± 0.04)mas and (-0.05 ± 0.03)mas using the mean and median of the differences, respectively.

In addition to the cluster parameters, all membership probabilities and individual stellar data are also made available, which can be useful for other research, as well as for the selection of targets for spectroscopy.

This paper is a follow-up to Monteiro et al. (2020). Both papers are part of an ongoing project to bring DAML into the Gaia era.

DATA AVAILABILITY STATEMENT

The data underlying this article, that support the plots and other findings, are available in the article and in its online supplementary material.

ACKNOWLEDGEMENTS

REFERENCES

An D., Terndrup D. M., Pinsonneault M. H., 2007, ApJ, 671, 1640
Arenou F., et al., 2017, A&A, 599, A50
Arenou F., et al., 2018, A&A, 616, A17
Barford N. C., 1967, Experimental Measurements: Precision, Error, and Truth. Addison-Wesley
Becker W., Fenkart R. B., 1970, in Becker W., Kontopoulos G. I., eds, IAU Symposium Vol. 38, The Spiral Structure of our Galaxy. p. 205
Bobylev V. V., Bajkova A. T., 2014, MNRAS, 437, 1549
Bossini D., et al., 2019, A&A, 623, A108
Bressan A., Marigo P., Girardi L., Salasnich B., Dal Cero C., Rubele S., Nanni A., 2012, MNRAS, 427, 127
Cantat-Gaudin T., Anders F., 2020, A&A, 633, A99
Cantat-Gaudin T., et al., 2018, A&A, 618, A93
Cantat-Gaudin T., et al., 2020, A&A, 640, A1
Capitanio L., Lallement R., Vergely J. L., Elyajouri M., Monreal-Ibero A., 2017, A&A, 606, A65
Cardelli J. A., Clayton G. C., Mathis J. S., 1989, ApJ, 345, 245
Carrera R., et al., 2019, A&A, 623, A80
Casamiquela L., et al., 2018, A&A, 610, A66
Castro-Ginard A., Jordi C., Luri X., Julbe F., Morvan M., Balaguer-Núñez L., Cantat-Gaudin T., 2018, A&A, 618, A59
Castro-Ginard A., Jordi C., Luri X., Cantat-Gaudin T., Balaguer-Núñez L., 2019, A&A, 627, A35
Castro-Ginard A., et al., 2020, A&A, 635, A45
De Silva G. M., et al., 2015, MNRAS, 449, 2604
Dias W. S., Lépine J. R. D., Alessi B. S., 2002a, A&A, 388, 168
Dias W. S., Alessi B. S., Moitinho A., Lépine J. R. D., 2002b, A&A, 389, 871
Dias W. S., Monteiro H., Caetano T. C., Lépine J. R. D., Assafin M., Oliveira A. F., 2014, A&A, 564, A79
Dias W. S., Monteiro H., Assafin M., 2018, MNRAS, 478, 5184
Dias W. S., Monteiro H., Lépine J. R. D., Barros D. A., 2019, MNRAS, 486, 5726
Donor J., et al., 2020, AJ, 159, 199
Ferreira F. A., Corradi W. J. B., Maia F. F. S., Angelo M. S., Santos J. F. C. J., 2020, MNRAS, 496, 2021
Gaia Collaboration et al., 2018a, A&A, 616, A1
Gaia Collaboration et al., 2018b, A&A, 616, A10
Georgy C., et al., 2013, A&A, 558, A103
Janes K., Adler D., 1982, ApJS, 49, 425
Kharchenko N. V., Piskunov A. E., Schilbach E., Röser S., Scholz R.-D., 2013, A&A, 558, A53
Kounkel M., et al., 2018, AJ, 156, 84
Krone-Martins A., Moitinho A., 2014, A&A, 561, A57
Lépine J. R. D., et al., 2011, MNRAS, 417, 698
Liu L., Pang X., 2019, ApJS, 245, 32
Maíz Apellániz J., Weiler M., 2018, A&A, 619, A180
Majewski S. R., et al., 2017, AJ, 154, 94
Moitinho A., 2001, A&A, 370, 436
Moitinho A., 2010, in de Grijs R., Lépine J. R. D., eds, IAU Symposium Vol. 266, Star Clusters: Basic Galactic Building Blocks Throughout Time and Space. pp 106–116 (arXiv:0911.1459), doi:10.1017/S1743921309990949
Moitinho A., Vázquez R. A., Carraro G., Baume G., Giorgi E. E., Lyra W., 2006, MNRAS, 368, L77
Monteiro H., Dias W. S., 2019, MNRAS, 487, 2385
Monteiro H., Dias W. S., Hickel G. R., Caetano T. C., 2017, New Astron., 51, 15
Monteiro H., Dias W. S., Moitinho A., Cantat-Gaudin T., Lépine J. R. D., Carraro G., Paunzen E., 2020, MNRAS, 499, 1874
Perren G. I., Giorgi E. E., Moitinho A., Carraro G., Pera M. S., Vázquez R. A., 2020, A&A, 637, A95
Riess A. G., et al., 2018, ApJ, 861, 126
Roeser S., Demleitner M., Schilbach E., 2010, AJ, 139, 2440
Salaris M., Cassisi S., 2006, Evolution of Stars and Stellar Populations. John

Wiley & Sons, Ltd

Sim G., Lee S. H., Ann H. B., Kim S., 2019, Journal of Korean Astronomical Society, 52, 145

Skrutskie M. F., et al., 2006, AJ, 131, 1163

Soubiran C., et al., 2018a, A&A, 619, A155

Soubiran C., et al., 2018b, A&A, 619, A155

Stassun K. G., Torres G., 2018, ApJ, 862, 61

Tarricq Y., et al., 2020, arXiv e-prints, p. arXiv:2012.04017

Taylor M. B., 2005, in Shopbell P., Britton M., Ebert R., eds, Astronomical Society of the Pacific Conference Series Vol. 347, Astronomical Data Analysis Software and Systems XIV. p. 29

Tolstoy E., Hill V., Tosi M., 2009, ARA&A, 47, 371

Vázquez R. A., May J., Carraro G., Bronfman L., Moitinho A., Baume G., 2008, ApJ, 672, 930

Zinn J. C., Pinsonneault M. H., Huber D., Stello D., 2019, ApJ, 878, 136

von Hippel T., Jefferys W. H., Scott J., Stein N., Winget D. E., De Gennaro S., Dam A., Jeffery E., 2006, ApJ, 645, 1436

APPENDIX A: LIST OF CLUSTERS WITH DISCREPANT AGES

APPENDIX B: LIST OF LIKELY NOT REAL CLUSTERS

This paper has been typeset from a TEX/LATEX file prepared by the author.

[!hb]

Table A1. List of 22 objects with differences out of 3σ in ages with Cantat-Gaudin et al. (2020).

Alessi 18	SAI 25	UBC 594
Barkhatova 1	UBC 276	UBC 668
Berkeley 1	UBC 322	
Berkeley 79	UBC 428	
COIN-Gaia 41	UBC 432	
FSR 1363	UBC 473	
Juchert 20	UBC 474	
LP 1218	UBC 491	
NGC 1977	UBC 521	
NGC 6664	UBC 548	

[!hb]

Table B1. List of objects that were found to likely not to be real open clusters. Clusters with the *fof* and *UBC* prefixes are from Liu & Pang (2019) and Castro-Ginard et al. (2020), respectively.

fof sc0160	fof sc0880	fof sc1467	fof sc1676	fof sc2175
fof sc0259	fof sc0888	fof sc1477	fof sc1688	fof sc2213
fof sc0317	fof sc0889	fof sc1481	fof sc1701	UBC 10b
fof sc0401	fof sc0895	fof sc1484	fof sc1702	UBC 625
fof sc0456	fof sc0988	fof sc1485	fof sc1703	UBC 649
fof sc0471	fof sc1024	fof sc1488	fof sc1712	
fof sc0611	fof sc1042	fof sc1514	fof sc1722	
fof sc0659	fof sc1052	fof sc1515	fof sc1723	
fof sc0660	fof sc1144	fof sc1537	fof sc1737	
fof sc0674	fof sc1148	fof sc1591	fof sc1752	
fof sc0692	fof sc1152	fof sc1605	fof sc1782	
fof sc0693	fof sc1154	fof sc1615	fof sc1811	
fof sc0730	fof sc1159	fof sc1627	fof sc2002	
fof sc0732	fof sc1210	fof sc1638	fof sc2004	
fof sc0736	fof sc1243	fof sc1649	fof sc2097	
fof sc0814	fof sc1245	fof sc1664	fof sc2112	
fof sc0834	fof sc1262	fof sc1665	fof sc2158	
fof sc0837	fof sc1305	fof sc1667	fof sc2167	
fof sc0841	fof sc1307	fof sc1670	fof sc2169	
fof sc0871	fof sc1308	fof sc1671	fof sc2173	

[!hb]

Table B2. List of objetcs that were found dubious open clusters. Clusters with the *fof* and *UBC* prefixes are from Liu & Pang (2019) and Castro-Ginard et al. (2020), respectively.

fof sc0253	fof sc0949	fof sc1547	fof sc1951	UBC 644
fof sc0396	fof sc0996	fof sc1548	fof sc1988	
fof sc0522	fof sc1026	fof sc1566	fof sc1999	
fof sc0559	fof sc1083	fof sc1574	fof sc2032	
fof sc0661	fof sc1084	fof sc1602	fof sc2035	
fof sc0696	fof sc1169	fof sc1637	fof sc2089	
fof sc0728	fof sc1176	fof sc1642	fof sc2155	
fof sc0743	fof sc1192	fof sc1668	fof sc2159	
fof sc0751	fof sc1194	fof sc1689	fof sc2160	
fof sc0809	fof sc1195	fof sc1711	fof sc2171	
fof sc0810	fof sc1202	fof sc1714	UBC 325	
fof sc0838	fof sc1203	fof sc1715	UBC 359	
fof sc0839	fof sc1208	fof sc1716	UBC 416	
fof sc0883	fof sc1225	fof sc1727	UBC 505	
fof sc0903	fof sc1239	fof sc1765	UBC 573	
fof sc0905	fof sc1385	fof sc1766	UBC 575	
fof sc0909	fof sc1387	fof sc1774	UBC 577	
fof sc0929	fof sc1428	fof sc1791	UBC 579	
fof sc0946	fof sc1452	fof sc1792	UBC 592	
fof sc0948	fof sc1461	fof sc1808	UBC 593	